Optical Interference Measurements of Interfacial Crack Initiation and Propagation

K. M. LIECHTI and Y. S. CHAI
Department of Aerospace Engineering and Engineering Mechanics, The University of Texas at Austin, Austin, TX 78712, USA

ABSTRACT

The development of a biaxial loading device for applying a wide range of mixed-mode loadings to an edge-cracked bimaterial strip is described. Crack initiation and propagation are examined on the basis of optical interference measurements of the crack opening displacements and complementary finite element analyses.

KEYWORDS

Interface crack initiation and propagation, crack opening interferometry, near tip opening displacements.

INTRODUCTION

The failure of interfaces is an inherently mixed-mode problem, particularly when cracks are constrained to grow along the interface. If composite materials or devices comprising two or more materials are to be designed to resist interfacial cracking then the criteria that govern initiation and growth under a range of mixed-mode conditions must be established. In some previous work (Trantina, 1972, Anderson et al., 1974, Mulville et al., 1978, Liechti et al., 1988), it was found that the critical value of energy release rate or toughness of the interface increased with increases in the Mode II component. In (Liechti et al., 1988) normal crack opening displacements were measured very close to the crack front region and indicated that the increase in toughness was due to increases in the extent of the region of inelastic material behavior surrounding the crack front as the Mode II component was increased. The purpose of this paper is to describe the development of a mixed-mode delamination tester that will allow a much wider range of mode-mixes to be examined. Results are presented for the initiation and transition to steady growth of cracks under one mode-mix ratio.

EXPERIMENTAL AND ANALYTICAL PROCEDURES

The specimen geometry that is being used for the study is an edge-cracked bimaterial strip (Fig.1). It is made of glass and epoxy with a teflon starter crack. It is clamped along the boundaries $y = \pm h$ and can be subjected to various combinations of bond-normal and bond-tangential displacements there. A linear elastic finite element analysis revealed (Fig.2) that, under these loadings, K_I and K_{II} were independent of crack length and the mode-mix ratio $\alpha = K_{II}^2/(K_I^2 + K_{II}^2)$ varied from 10% to 90% under tensile bond normal and bond-tangential applied displacements, respectively. In the previous work, (Liechti et al., 1988), $0.10 < \alpha < 0.25$. The loads are applied by a specially developed mixed-mode delamination tester shown schematically in Figure 3. The actuators are microstepping stepper motors acting through preloaded ball screws to provide $0.2\mu m$/step. The movement of the grips is sensed by linear optical encoders whose signals are used for feedback control by an IBM PC-AT. The linear bearings are used to react loads in one direction while allowing orthogonal movement in the other. In addition to measuring loads and displacements across the interface, normal crack opening displacements (NCOD) are measured in the crack front region using crack opening interferometry. Since viewing is made through the glass perpendicular to the plane of the interface, the method is very useful for assessing three dimensional effects, i.e., extent of crack front curvature, its regularity etc. In the present arrangement the NCOD measurements are made over a $500\mu m$ field of view. The fringes can be located to within $5\mu m$ and each dark/bright fringe transition corresponds to an increment in NCOD of $0.13\mu m$. The fringe patterns are recorded through a high resolution video system which includes a video timer for synchronization with measurements of load and applied displacement. The subsequent analysis of fringe patterns has been fully automated using a digital image analysis system that captures and digitizes and stores an intensity profile every thirtieth of a second. The loading device and crack opening interferometry apparatus are shown in Figure 4.

The NCOD by themselves are not sufficient for determining mixed-mode fracture parameters and criteria and so the NCOD data are complemented by linear elastic, plane strain analyses using the finite element code VISTA (Becker et al., 1984). The crack tip region is modeled by special singular elements (Stern, 1979) which capture the square root and linear terms in the displacement fields. Mode I and Mode II stress intensity factors are extracted by a conservation integral approach (Yau et al., 1984). For a particular experiment, measurements of crack length and applied displacements are used to obtain solutions for NCOD which are compared with measured values taken from a central scan of the fringe patterns. If the NCOD match, then the finite element solution is used to extract fracture parameters.

RESULTS

A series of experiments under bond-normal loading have been conducted. The first step was to compare the predicted and measured values of NCOD close to the crack front. An example of such a comparison is shown in Figure 5 where the measurements are the discrete points and the various lines are the finite element solutions at corresponding load levels. The NCOD measurements indicate that there is always some initial crack opening for a zero value of bond-normal applied displacement, v_o, at the beginning of an experiment. In order to make comparisons at higher loads the initial gap was introduced to the finite solution by applying a fictitious bond-normal loading to the appropriate

level. The finite element solutions for $v_o \geq 0$ are shown as the lines, with the full line representing the NCOD solution for the bond-normal displacements associated with the onset of propagation, v_{o_c}. It can be seen that there is very reasonable agreement between predictions and measurements up to initiation. Far away from the crack front, the predicted values of NCOD are slightly lower than the measured ones. It was found that this degree of agreement could only be obtained when the relative movement of the grips was measured across the interface using miniature capacitative devices instead of relying on the data from the linear encoders. There is apparently some compliance in the grips which, in conjunction with the placement of the optical encoders, magnifies the relative movement across the grips. In view of the results of Figure 5, values of K_I and K_{II} corresponding to a particular measured NCOD profile were obtained from finite element solutions whose NCOD had been matched with the measured values 200 to $400\mu m$ from the crack front, well removed from any inelastic effects.

Previous work (Liechti et al., 1988) had shown that inelastic effects in NCOD were more apparent when the profiles were plotted logarithmically. Although the effects are not so dramatic for the bond-normal loading case ($\alpha = 0.10$) considered here there were some notable changes in the profiles as the crack initiated and then established a steady velocity. The logarithmic profiles for one experiment are shown in Figure 6 for the zero state, initiation ($\Delta a/a = 2 \times 10^{-4}$) and when the crack had attained a steady speed. The profile at zero and low loads (not shown) is quite linear with a slope, $m_E = 0.521$, that reflects mainly the square root and a smaller linear component in the linear elastic, small strain near tip expansion for displacements in terms of distance from the crack front. At higher loads, the profiles have a bilinear appearance reflecting regions of elastic response ($m_E = 0.521$) and inelastic response ($m_p = 0.426$ for $v_o/v_{o_c} = 1.0$). The straightness of the data in the inelastic region suggests that the NCOD there have a power law dependence on the distance from the crack front. The fact that the slope is less than 0.5 indicates a stronger singularity in strain in the inelastic region. Far away from the crack front, the profiles of the critical case and the steadily propagating crack are indistinguishable. However, as the crack front is approached there is a dip in the propagating crack profile before a linear section is established very close to the crack front. The region of the dip corresponds to the location of the original stationary crack front which always seems to leave a discontinuity in the NCOD profiles as the propagating crack front moves away. The slope of the linear section very close to the crack front was $m_p = 0.380$, lower than the corresponding value for the critical case, indicating a difference in the singular behavior from initiation to propagation.

The values of the slopes of the elastic and inelastic profiles are noted at various degrees of crack extension in Figure 7 where the resistance energy release rate is plotted as a function of crack extension. The values of the elastic slope are noted above the G-curve and were constant throughout. The inelastic slope values are shown below the G-curve and increase before decreasing to a steady value $m_p = 0.38$. From the times noted at the top of the plot it can be seen that initiation ($da/a = 2 \times 10^{-4}$) occurred 108.5 seconds after load initiation and the velocity was quite steady thereafter. The plastic zone size (taken as the intersection of the linear portions of the profiles) increased sharply up to initiation and then dropped off to a steady value as the crack propagated steadily. The values of energy release rate shown in Figure 7 were derived from finite element solutions whose NCOD had been matched with the measured values in the regions of elastic response. The G values increase until initiation and remain quite steady thereafter. In view of the fact

that they were derived from NCOD profiles in regions of elastic response, both initiation and propagation are therefore essentially characterized by the same elastic NCOD profile. Thus the noted differences closer to the crack front do not have much effect, because, as the estimates of the plastic zone indicate, the zones of inelastic behavior are quite small so that small scale yielding considerations should apply. Nonetheless, as the mode-mix ratio is increased, the extent of inelastic behavior increases (Liechti et al., 1988) so that similarity is lost and the adhesive fracture toughness becomes a function of mode-mix. It remains to be seen just how large the inelastic zones are under the very high mode-mix ratios that can be obtained with the mixed-mode delamination tester developed here.

The repeatability of the results for the same value of mode-mix was established by conducting a series of experiments on the same specimen by arresting and reinitiating the crack a number of times. The features described above were observed in all experiments. A critical fracture resistance or toughness, G_c , was defined as the nearly constant value associated with initiation and propagation. The values of G_c for each experiment are shown in Figure 8 where it can be seen that the repeatability is good. The dashed line represents an average value of 0.097 in lb/in^2 (16.98 J/m^2) as the toughness of this glass epoxy system for $\alpha = 0.10$.

CONCLUSIONS

A mixed-mode delamination tester has been developed that is capable of applying a large range of mixed-mode conditions for interface cracks. The device was used to examine crack initiation and propagation under bond-normal applied displacements which provided a relatively low mode-mix ratio of 10%. Measurements of NCOD were made quite close to the crack front. They revealed differences in the extent and character of the regions of inelastic material behavior that were associated with initiation and steady propagation. The regions of inelastic behavior were small and initiation and propagation were governed by the same elastic NCOD profile or energy release rate. A series of experiments established the repeatability of the fracture resistance determined in this way.

REFERENCES

1. Trantina, G.G. (1972). Combined Mode Crack Extension in Adhesive Joints. *J. Comp. Matls.*, 6, 371–385.

2. Anderson, G.P., K.L. DeVries and M.L. Williams (1974). Mixed Mode Stress Field Effect in Adhesive Fracture. *Int. J. of Fracture*, 10, 565–583.

3. Mulville, D.R., D.L. Hunston and P.W. Mast (1978). Developing Failure Criteria for Adhesive Joints Under Complex Loading. *J. Eng. Mat. Tech.*, 100, 25–31.

4. Liechti, K.M. and E.C. Hanson (1986). Nonlinear Effects in Mixed-Mode Interfacial Delamination. *Int. J. Fracture*, 36, 199–217.

5. Becker, E.B., R.S. Chambers, L.R. Collins, W.G. Knauss, K.M. Liechti and J. Romanko (1984). Viscoelastic Stress Analysis Including Moisture Diffusion for Adhesively Bonded Joints. Air Force, Wright Aeronautical Lab. Report No. AFWAL-TR-84-4057.

6. Stern, M. (1979). Families of Consistent Conforming Elements with Singular Derivative Fields. *Int. J. for Num. Meth. in Eng.*, 14, 409–421.

7. Yau, J.F. and S.S. Wang (1984). An Analysis of Interface Cracks between Dissimilar Isotropic Materials Using Conservation Integrals in Elasticity. *Eng. Fract. Mech.*, 20, 423–432.

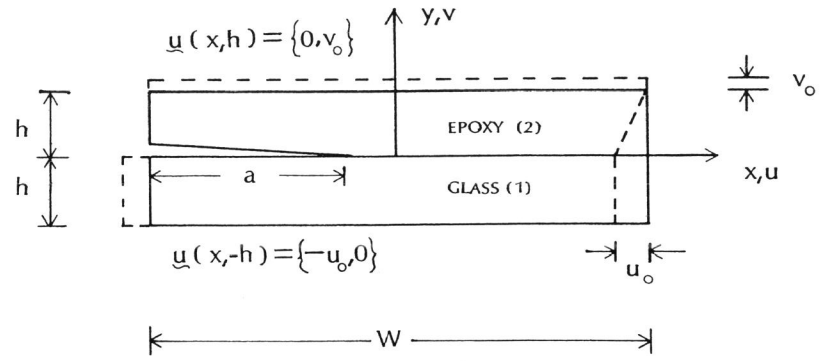

Fig. 1. Edge-cracked bimaterial strip specimen.

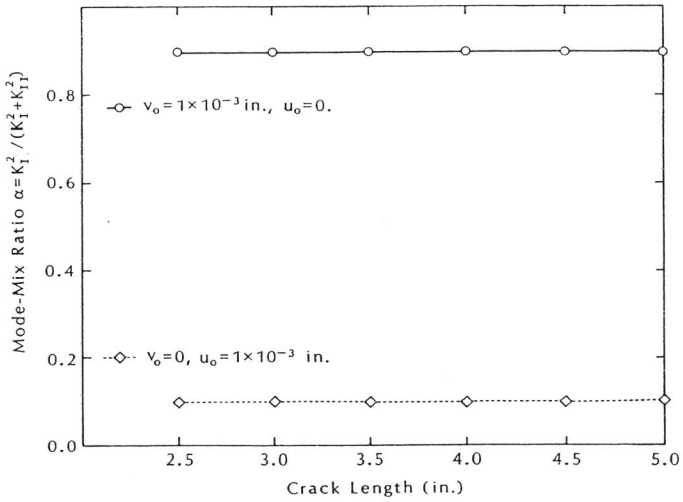

Fig. 2. Mode-mix ratios under bond-normal and bond-tangential applied displacements.

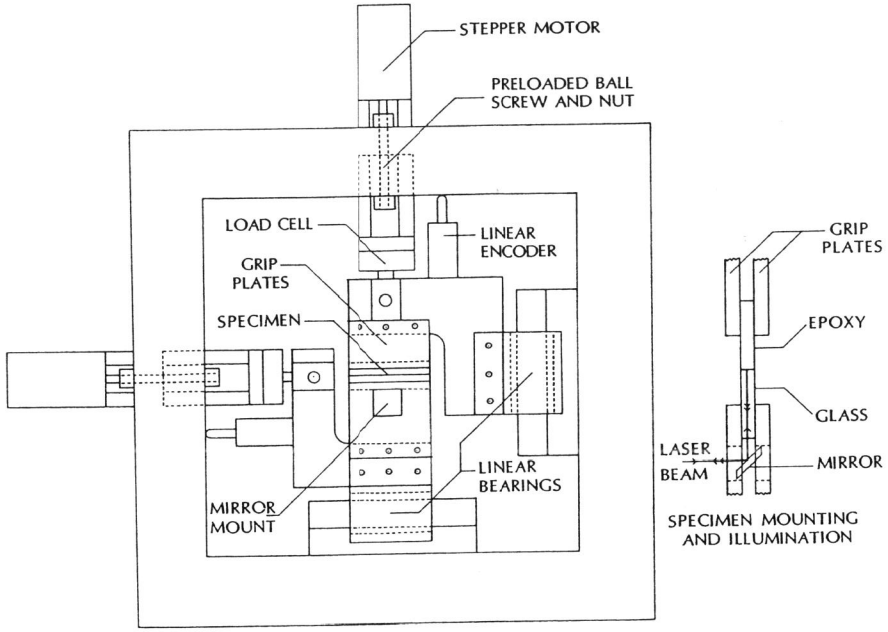

Fig. 3. Schematic of mixed-mode delamination tester.

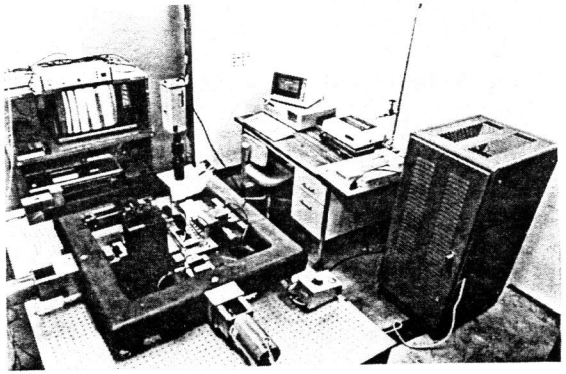

Fig. 4. Mixed-mode delamination tester with crack opening interferometry apparatus.

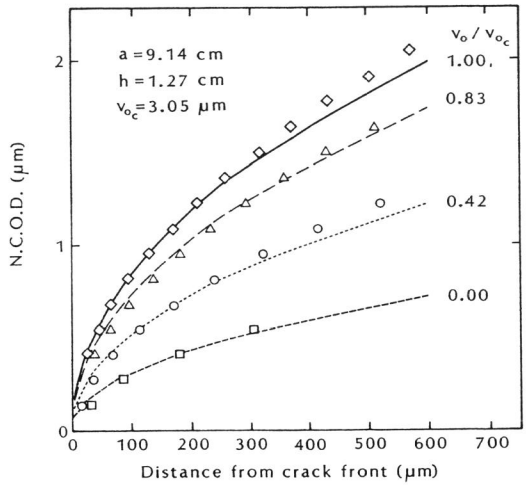

Fig. 5. Comparison of predicted and measured NCOD profiles under bond-normal loading.

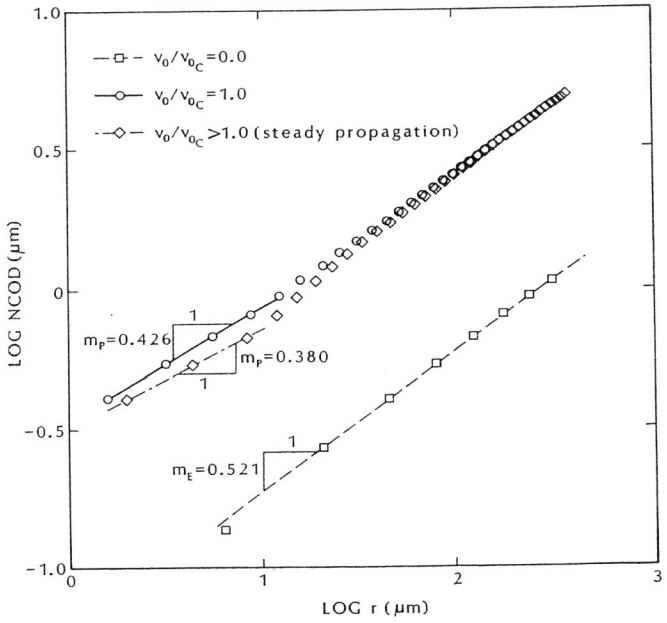

Fig. 6. Crack front asymptotics.

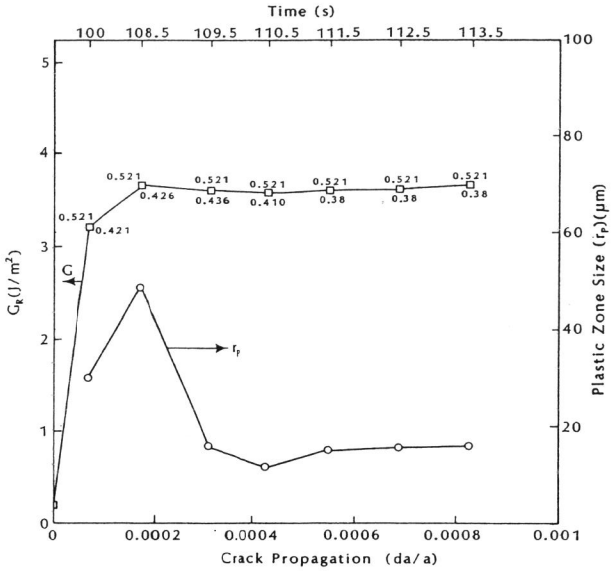

Fig. 7. Crack extension behavior.

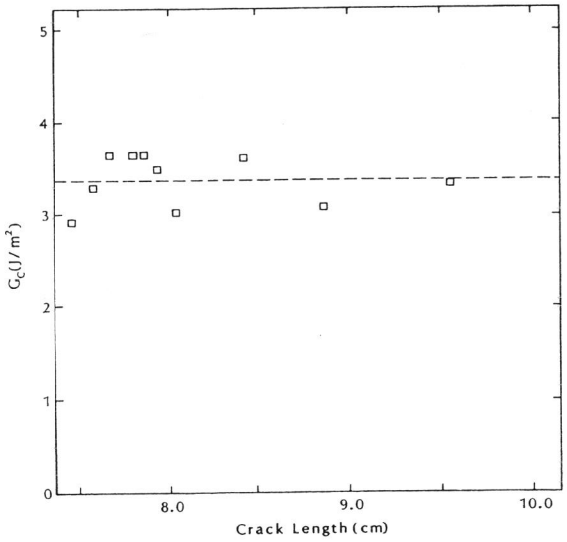

Fig. 8. Critical fracture resistance.